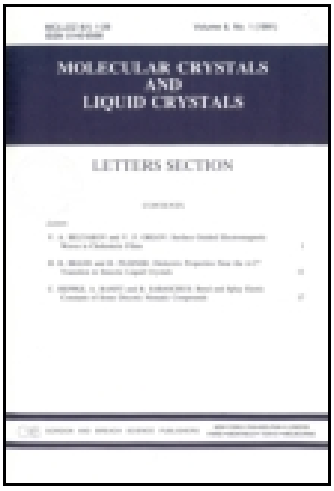

Molecular Crystals and Liquid Crystals
Publication details, including instructions for authors and subscription information:
http://www.tandfonline.com/loi/gmcl20

Fabrication and Crystal Structure Analysis of a CIGS Solar Cell Absorber by Thermal Annealing of Sputtered CIG Precursors Deposited with a Se Layer

Yong Bae Kim[ac], You Na Lee[a], Seung Iel Park[b] & Jung-Hee Lee[c]
[a] Photovoltaic Technology Research Team, Gumi Electronics & Information Technology Research Institute, Gumi 730-853, Korea
[b] Sukwon Co., Ltd., Gumi-si, Gyeongsangbuk-do, 136-791, Korea
[c] The School of Electrical Engineering and Computer Science, Kyungpook National Univ., Daegu, 712-714, Korea
Published online: 06 Dec 2014.

To cite this article: Yong Bae Kim, You Na Lee, Seung Iel Park & Jung-Hee Lee (2014) Fabrication and Crystal Structure Analysis of a CIGS Solar Cell Absorber by Thermal Annealing of Sputtered CIG Precursors Deposited with a Se Layer, Molecular Crystals and Liquid Crystals, 602:1, 244-250, DOI: 10.1080/15421406.2014.944785

To link to this article: http://dx.doi.org/10.1080/15421406.2014.944785

Mol. Cryst. Liq. Cryst., Vol. 602: pp. 244–250, 2014

ISSN: 1542-1406 print/1563-5287 online
DOI: 10.1080/15421406.2014.944785

Taylor & Francis
Taylor & Francis Group

Fabrication and Crystal Structure Analysis of a CIGS Solar Cell Absorber by Thermal Annealing of Sputtered CIG Precursors Deposited with a Se Layer

YONG BAE KIM,[1,3,*] YOU NA LEE,[1] SEUNG IEL PARK,[2] AND JUNG-HEE LEE[3]

[1]Photovoltaic Technology Research Team, Gumi Electronics & Information Technology Research Institute, Gumi, Korea
[2]Sukwon Co., Ltd., Gumi-si, Gyeongsangbuk-do, Korea
[3]The School of Electrical Engineering and Computer Science, Kyungpook National Univ., Daegu, Korea

Various Cu(In,Ga)Se_2 (CIGS) films were prepared by using in-line sputter for CIG precursor and evaporator for selenization. Deposition parameters are substrate temperature at sputtering process, post annealing temperature (400∼500°C) and annealing method (thermal furnace and high-temperature in-situ XRD). Temperature dependent XRD patterns of the samples were measured with high temperature option and this pattern shows that post annealing at 400∼500°C is necessary for CIGS absorber deposition with no second phase by in-line sputtering. The CIGS film which is annealed at 500°C shows good crystallographic property and there is no second phase like $Cu_{2-x}Se$.

Keywords CIGS absorber; sputtering; CIG ternary targets; post annealing

Introduction

Chalcopyrite ternary compound Cu(In,Ga)Se_2 (CIGS) have been paid attention to be a promising absorber material for a high conversion efficiency solar cell which have very high potential with long-term durability and low production cost. 20% conversion efficiency, which is the highest, was reported for CIGS material deposited by so-called three-stage co-evaporation method [1]. However, the conventional co-evaporation methods have disadvantages such as high costs in production and difficulties in scaling up, which must be solved before the commercialization of the large scale manufacturing of CIGS solar cells [2].

In this work, Mo and Cu(In,Ga)(CIG) were deposited by in-line sputter on soda-lime glass (SLG) substrate and Se by evaporation in order to derive optimal parameters such as post annealing temperature, compositions of CIG target and crystal structure of CIGS absorber material in a large scale manufacturing process.

*Address correspondence to Yong Bae Kim, Photovoltaic Technology Research Team, Gumi Electronics & Information Technology Research Institute, Sandong-myeon, Gumi-si, Gyeongsangbuk-do 730-853, Korea (ROK). E-mail: ybk@geri.re.kr

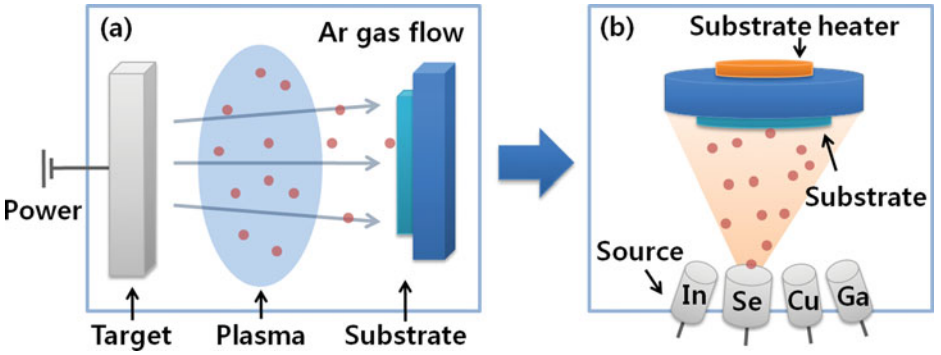

Figure 1. Schematic diagram of (a) in-line sputter and (b) selenization chamber.

Experimental

Newly developed in-line sputter for CIGS solar cell was used to deposit back contact (Mo) and absorber (CIGS). Since there are bonding problem for large scale Se sputter target, we used co-evaporator for selenization. Figure 1 shows schematic diagram of in-line sputter and co-evaporator. The working pressure of in-line sputter is usually 1×10^{-3} Torr, and substrate can be heated up to 800°C. The co-evaporator has 5 individual cells and can deposit simultaneously but we used only Se effusion cell in this work and also the substrate can be heated up to 900°C.

Soda-lime glass(SLG) which has 10×10 cm^2 size and 1 mm thickness was used for substrate material. Mo deposited on SLG at 200°C substrate temperature and 4 kW sputter power. Mo film has 0.4 μm thickness and 0.25Ω/□ sheet resistance. CIG precursor deposited by in-line sputter at 150°C substrate temperature. Table 1 shows deposition condition of various samples.

Table 1. Deposition and annealing conditions of samples. All samples have same condition except post-annealing temperature

Element layer specifications			Post-annealing			Sample No.
Material	Deposition method	Condition	Condition		Temperature	
Mo	RF magnetron sputter	1st layer : 250°C, 2nd layer : 25°C, Power : 4kW	Working pressure	1.9×10^{-2} Torr	400°C	C400
					420°C	C420
CIG		25°C, 0.8kW	Glass cover	Used	450°C	C450
Se	Thermal evaporator	300°C, 22min	Temperature holding time	30min	500°C	C500

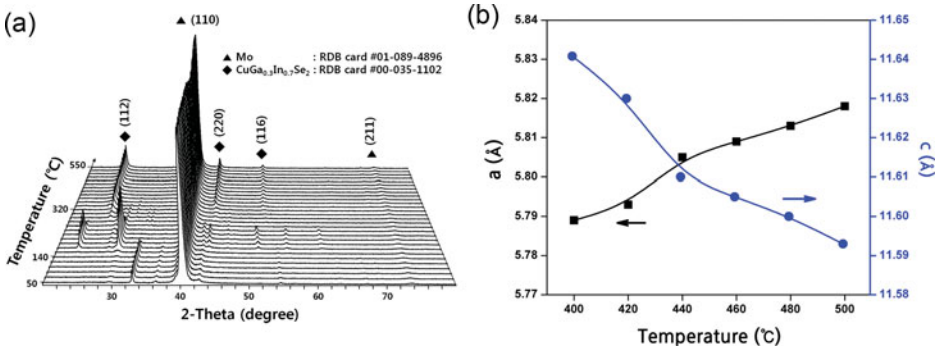

Figure 2. (a) Temperature dependent XRD measurement result. (b) Lattice parameter (a and c axis) calculation in the temperature range 400°C to 500°C. The curve in (b) is a guideline (by B-Spline fitting) for eye.

FE-SEM & EDS (JEOL 7000 model) was used for surface and cross-sectional profile measurement. Thermogravimetric analysis (TGA, TA Instruments Inc. SDT Q600 model) was used to measure weight change of CIGS samples to get post annealing temperature. X-ray diffraction data were collected by a D/MAX-2500 Rigaku diffractometer with Cu-Kα radiation ($\lambda_\alpha = 1.54256$Å) at various temperatures to analyze the crystal structure of CIGS. Raman spectroscopy (Renishaw InVia model) was used to investigate presence of second phase with excitation wavelength from 514 nm to 785 nm. High resolution glow discharge mass spectrometer (GDS, Thermo Fisher Scientific Element GD model) was used for the elemental analysis of the samples with abundance sensitivity around 7 ppm.

Results and Discussion

To investigate the starting temperature of CIGS crystallization, we measured temperature dependent in-situ XRD of CIGS sample which was not post annealed (Figure 2). Indium

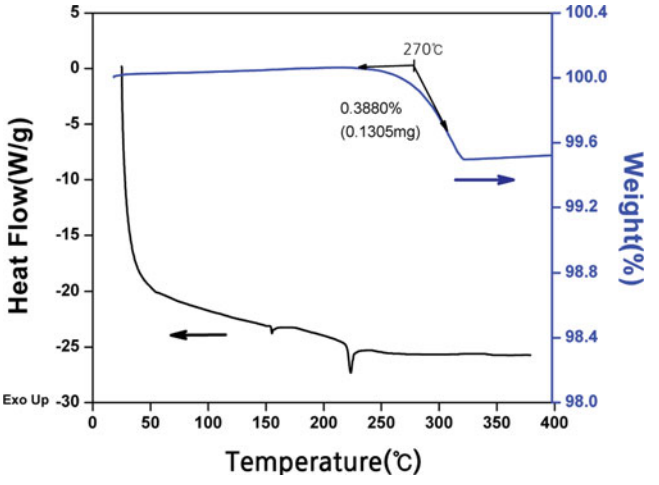

Figure 3. Thermogravimetric analysis by TGA and heat flow measurement by DSC.

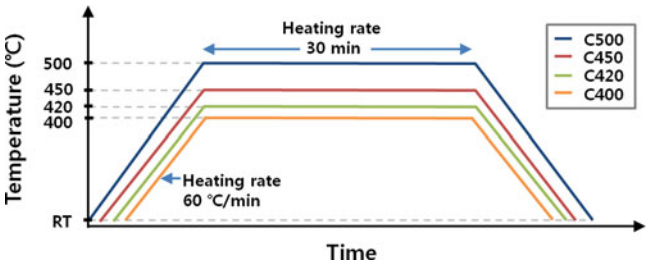

Figure 4. Time versus temperature graph for the post annealing condition.

reflection peak appears at temperature range from room temperature to 160°C and Se reflection peak also appears from 140°C to 260°C. CIGS XRD reflection peak starts at 280°C but fully crystallized peak with no second phases and peak broadening starts at 400°C (Figure 2(a)). Figure 2(b) shows temperature dependent change of lattice parameter of CIGS which has a tetragonal I-42d (crystallographic space group number 122) structure. As the temperature increasing, lattice parameter a(a-axis) increases while c(c-axis) decreases (Figure 2(b)). Thermogravimetric analysis of CIGS (Figure 3) also shows dramatic weight loss of about 0.4% at about 300°C and exothermic heat flow at around 230°C. As we noted before, Se peak start to disappear at 260°C and CIGS peak shows at 280°C in in-situ XRD

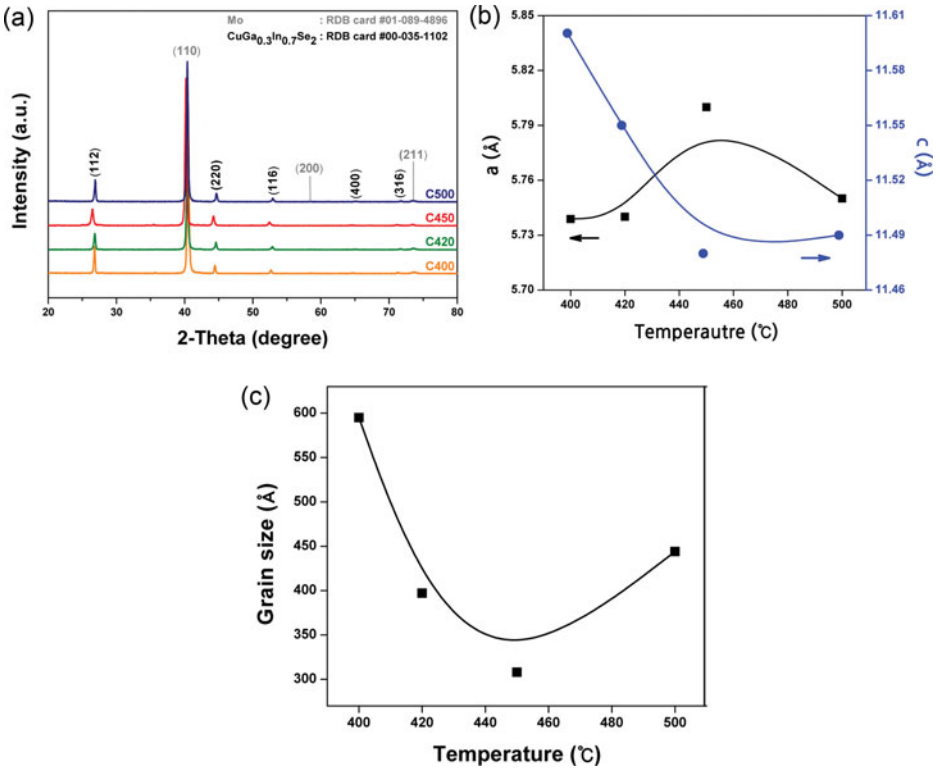

Figure 5. (a) XRD measurement result. (b) Lattice constant calculation. (c) Grain size calculation. The curve in (b, c) are guidelines (by B-Spline fitting) for eye.

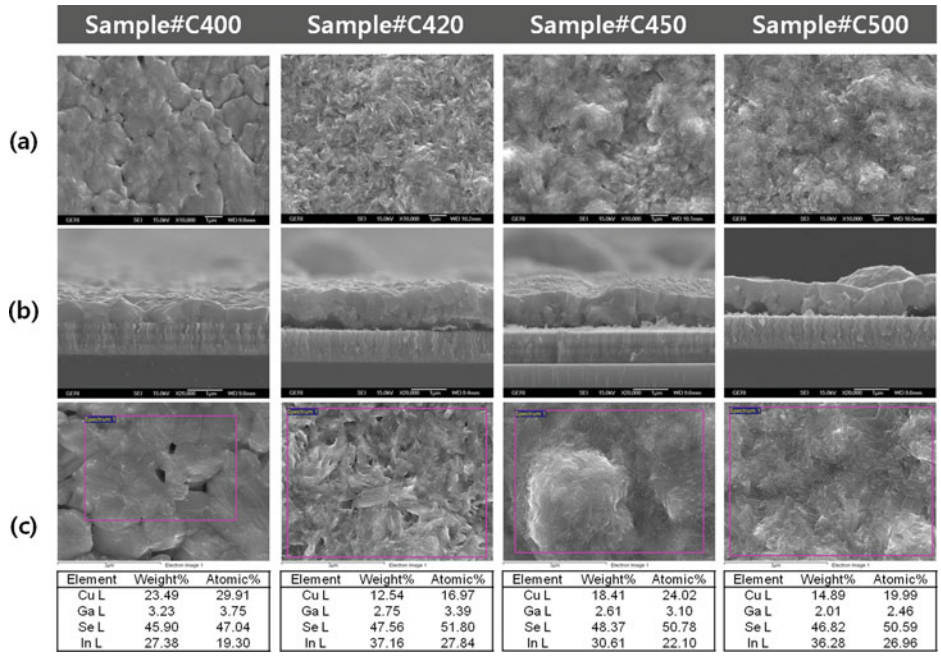

Element	Weight%	Atomic%
Cu L	23.49	29.91
Ga L	3.23	3.75
Se L	45.90	47.04
In L	27.38	19.30

Element	Weight%	Atomic%
Cu L	12.54	16.97
Ga L	2.75	3.39
Se L	47.56	51.80
In L	37.16	27.84

Element	Weight%	Atomic%
Cu L	18.41	24.02
Ga L	2.61	3.10
Se L	48.37	50.78
In L	30.61	22.10

Element	Weight%	Atomic%
Cu L	14.89	19.99
Ga L	2.01	2.46
Se L	46.82	50.59
In L	36.28	26.96

Figure 6. (a) SEM image of the surface. (b) Cross-sectional image. (c) EDS results.

patterns. For reasons mentioned above, we can infer that the crystallization of CIGS starts at around 230°C and Se atoms starts to participate in the CIGS composition at the same time from in-situ XRD, TGA, and heat flow results comprehensively. Finally, we selected post annealing temperature at 400°C (sample number C400), 420°C (C420), 450°C (C450) and 500°C (C500).

Figure 4 shows temperature versus time diagram. Typical heating rate was 60°C/min. At the cooling stage, there is intermediate region at 280°C to get good interface between Mo and CIGS.

Figure 5(a) shows XRD data of post annealed samples. All samples are identified to have tetragonal crystallographic space group number 122 and show CIGS reflections peaks. The lattice parameter a (a-axis) slightly increases from 5.74Å to 5.8Å with increasing post annealing temperature (Figure 5(b)). But for the C500 sample, goes down to 5.75Å. This result shows that the increment of post annealing temperature affects a-axis broadening and has parabolic behavior with maximum point at around 450°C. But c-axis grows smaller with increasing temperature and finally reaches to stable stage at 500°C. Also c-axis shows parabolic behavior with minimum point at around 450°C. This behavior shows that there is crystallographically meta-stable point at around 450°C and C500 sample (annealed at 500°C) has good CIGS crystal quality. This results show similar behavior except parabolic curve maximum (a-axis) and minimum (c-axis) which may be because of measuring temperature. An estimate of the average grain size, δ, of samples was made using Eq. (1) and the FWHMs of the XRD peaks for different orientations.

$$\delta = 0.9\lambda/\mathrm{FWHM}(\cos\theta) \tag{1}$$

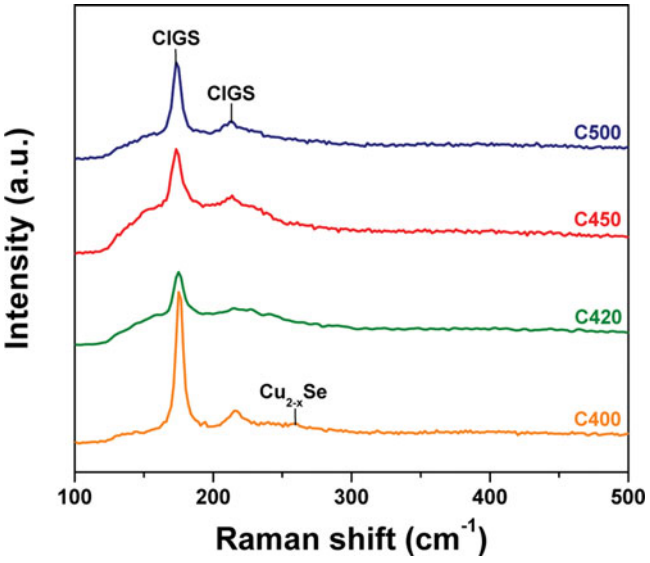

Figure 7. Raman spectra of the samples.

where δ (Å), λ (Å), and FWHM are grain size, wavelength of the x-ray source (Cu-Kα), and full width at half maximum, respectively. Grain size is about 45 nm at 500°C which slightly bigger than 40 nm at 450°C and also shows parabolic behavior with minimum at 450°C (Figure 5(c)).

Surface profile measurements in Figure 6 show that grain size is dependent on post annealing temperature which is in accordance with the grain size calculation by XRD measurement (Figure 5(c)). Cross-sectional profile also shows same tendency to grain size. The interface between CIGS and Mo shows good interconnection except C400 and C420 samples. By stoichiometric analysis with EDS in Figure 6(c), sample C500 has $Cu_{1-x}In_{0.7}Ga_{0.3}Se_2$ where $x \sim 0.1$. It is well-known that the CIGS with $E_g \sim 1.2$eV and lattice constant (a-axis) $\sim$ 5.7Å shows good conversion efficiency. C500 sample (a $\sim$

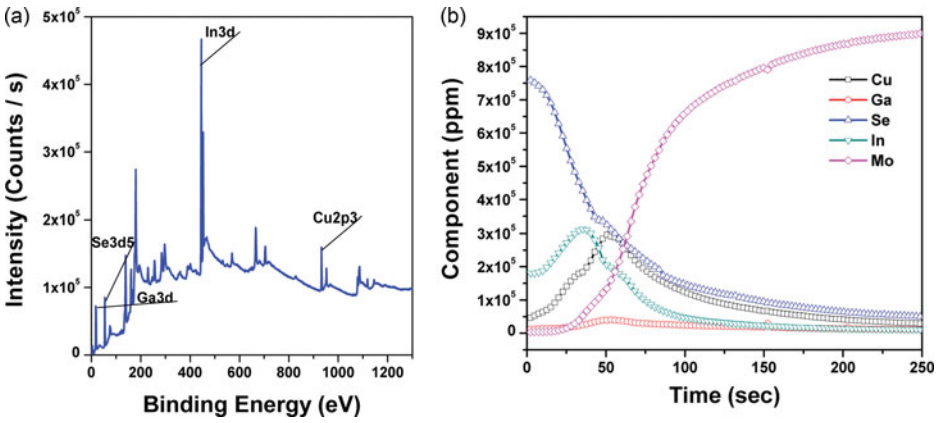

Figure 8. (a) XPS spectra and (b) GDS spectra of C500 sample.

5.73Å) has a comparable lattice constant value ∼ 5.7Å and Cu-poor (Cu/(In + Ga) ∼ 0.9) stoichiometry. So C500 seems to have good CIGS crystal property to show good conversion efficiency [3].

Raman spectroscopic measurement (Figure 7) shows that there is CIGS peak for all samples and the $Cu_{2-x}Se$ peak which is second phase decreases with increasing post annealing temperature and finally there is no peak for sample C500 [4]. The power was 200 mW(10% of full power) and the spot size of the laser was 0.2 mm.

We measured XPS spectra and GDS to verify that CIGS of C500 sample crystallized properly (Figure 8). Cu 2p, In 3d, Ga 3d, and Se 3d peaks were identified in the spectrum and the binding energy was 932.22, 445.04, 18.32, and 54.9 eV, respectively (Figure 8(a)). From the GDS result, it is obvious that, Se and In atoms are abundant at the surface and every atom of CIGS properly exists (Figure 8(b)).

Conclusions

In this work, various CIGS samples depending on the post annealing temperature were analyzed to get appropriate thermal annealing condition in CIGS in-line sputter process for large-scale manufacturing. C500 with post annealing temperature 500°C shows good crystallographic property and there is no second phase like $Cu_{2-x}Se$. For in-line sputter process, 500°C is somewhat high temperature condition but is necessary to get suitable CIGS absorber layer to show high conversion efficiency.

Funding

This work was supported by the Center for Science & Technology Research (CSTR) grant funded by the Korean government (MEST). CSTR-001-100701-03.

References

[1] Ingrid, Repins, Miguel, A., Contreras, Brian Egaas, Clay, DeHart, John, Scharf, Craig, L., Perkins, Bobby To, and Rommel, Noufi. (2008). *Prog. Photovolt : Res. Appl.*, *16*, 235239.
[2] Tokio, Nakada, Kazuo, Migita, Shigeru, Niki, & Akio, Kunioka. (1995). *Japanese Journal of Applied Physics*, *34*, 4715.
[3] Han, Sung-Ho, Hasoon, Falah S., Pankow, Joel W., Hermann, Allen M., & Levi, Dean H. (2005). *Applied Physics Letters*, *87*, 151904.
[4] Chen, Chia-Hsiang, Lin, Tzu-Ying, Hsu, Chia-Hao, Wei, Shih-Yuan, & Lai, Chih-Huang. (2013). *Thin Solid Films*, *535*, 122